Supporting Information

Comprehensive and Accurate Analysis of Working Principle in Ferroelectric Tunnel Junction Using Low-frequency Noise Spectroscopy

Wonjun Shin[1]†, Kyung Kyu Min[1,2]†, Jong-Ho Bae[3]†, Jiyong Yim[4], Dongseok Kwon[1], Yeonwoo Kim[1], Junsu Yu[1], Joon Hwang[1], Byung-Gook Park[1], Daewoong Kwon[4]*, and Jong-Ho Lee[1]*

[1]Department of Electrical and Computer Engineering and Inter-university Semiconductor Research Center, Seoul National University, Seoul 08826, Republic of Korea.

[2]SK Hynix Inc., Icheon 17336, Korea.

[3]School of Electrical Engineering, Kookmin University, Seoul 02707, Korea.

[4]Department of Electrical Engineering, Inha University, Incheon, Korea.

†W. Shin, K. Min, and J. Bae contributed equally to this work.

* Corresponding author.

* dw79kwon@inha.ac.kr (D. Kwon)

* jhl@snu.ac.kr (J.-H. Lee)

This PDF file includes:

Supplementary Text

Figs. S1 to S9

S1 – LFN measurement

We use a semiconductor parameter analyzer (B1500A), low noise current amplifier (SR570), and signal analyzer (35670A) to measure power spectral density. The measurement process is explained as follows: The voltage applied to the TiN was supplied by the B1500A. The output current of the FTJ was connected to the SR570, converting the current fluctuation into a voltage fluctuation. 35670A converts the dynamic signal from SR570 to a power spectral density (fig. S2A). The positive V_{SET} and negative V_{RESET} are applied for the set time (t_{SET}) to measure the power spectral density of the FTJ in the LRS and HRS, respectively. After the V_{SET} and V_{RESET} are applied, the V_{READ} is applied to the TiN to measure the power spectral density. The V_{READ} is varied from 1.5 to 4.0 V.

1) Noise floor

It is important to determine the noise floor of the measurement system. The current amplifier has a noise floor of 4×10^{-27} in low noise mode (SR 570 Manufacturer specifications). Fig. S3C shows the power spectral density of the measurement system in low noise mode, which coincides with manufacturer specification. This value is much lower than the device noise, which guarantees that the power spectral densities measured in this work are not affected by the noise floor of the measurement system.

2) Measurement bandwidth

There might be a spectral distortion of the power spectral density of the devices due to the limited bandwidth of the circuit. The internal circuitry in SR570 preserves the amplitude of the signal and phase. In low noise mode, the rated bandwidths of the SR570 are 2, 20, and 200 kHz with sensitivities of 100 nA, 1 μA, and 10 μA, respectively. Therefore, there would be no spectral distortion, given the limited frequency range in this work ($f \leq 1.6$ kHz for HRS and $f \leq 20$ kHz for LRS). Note that the sensitivity of a 100 nA is only used for measuring the power spectral density of the FTJ in the LRS with low V_{READ}.

S2 – LFN characteristics of the RRAM

We compare the LFN characteristics of the FTJ with RRAM. The FTJ and RRAM are 2-terminal memory devices whose state (LRS or HRS) can be modulated by the V_{SET}. However, their working principles are different, which requires a systematic comparison. The fabricated RRAM has its structure of metal-insulator-metal (MIM) structure. TiN of 1000 Å is used as bottom and top electrodes, and HfO_x of 6 nm is deposited therebetween. The materials used for each process were identical to the FTJ stack in text, which guarantees a fair comparison between the RRAM and FTJ. Note that the post-deposition annealing condition of RRAM is different from that of FTJ: Rapid thermal annealing with 650 ^{o}C, 30 s was applied to the MIM stack for characteristics optimization.

The conduction mechanisms of the metal-oxide-based RRAM are relatively well known compared to FTJ. Fig. S3A shows a typical current-voltage (*I*-*V*) curve of the RRAM. The voltage was applied to the top electrode and the bottom electrode as grounded in this measurement. When

the voltage is swept from 0V to positive, RRAM is switched from HRS to LRS. Note that a compliance current of 200 μA is applied to protect the device from hard breakdown. The LRS remains during the voltage sweep back to negative bias, and RESET appeared in $V_{RESET.}$ The switching operation of the HfO_x-RRAM can be explained by the formation and rupture of conductive filament.[58,59] When the positive V_{SET} was applied, the oxygen vacancies in the HfO_x were re-arranged, and the conductive filament was formed, resulting in LRS. The abruptly increased current in the positive sweep direction in Fig. S3A depicted this resistivity switching situation. On the contrary, When the negative V_{RESET} was applied, the oxygen ion is recombined to the oxygen vacancies and finally ruptures the conductive filament, resulting in HRS.

The LFN characteristics of the RRAM can be explained in conjunction with conduction mechanisms. In the case of the LRS, the filled trap sites act as a conductive filament, resulting in $1/f$ noise behaviors (Figure S3b). During the reset process, the conductive filament is ruptured, and charges tunnel through trap sites to find the shortest distance between the top and bottom electrodes. Accordingly, the $1/f$ noise of the RRAM in the HRS shows a much larger noise and the Lorentzian behavior in the spectral density is observed due to the TAT (Figure S3b).

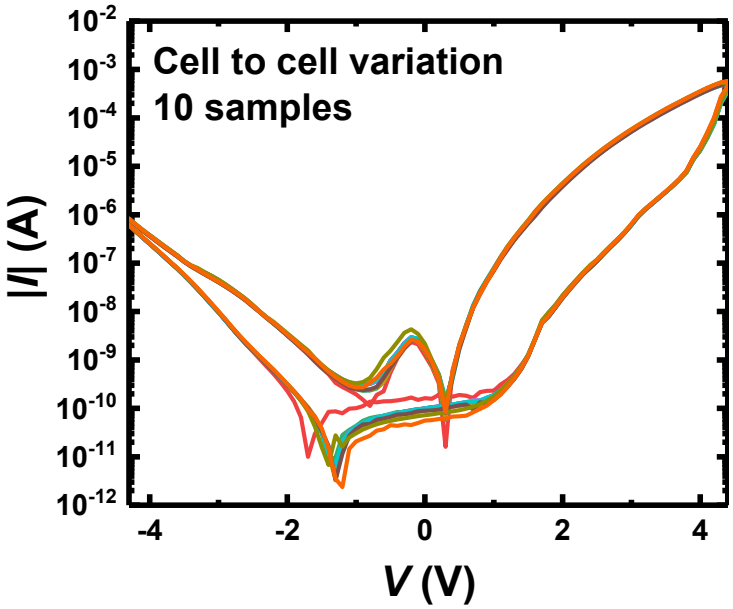

Figure S1. Cell to cell variation. Hysteresis curves ($|I|$-V) of the 10 independent samples. The fabricated FTJ shows excellent cell to cell uniformity.

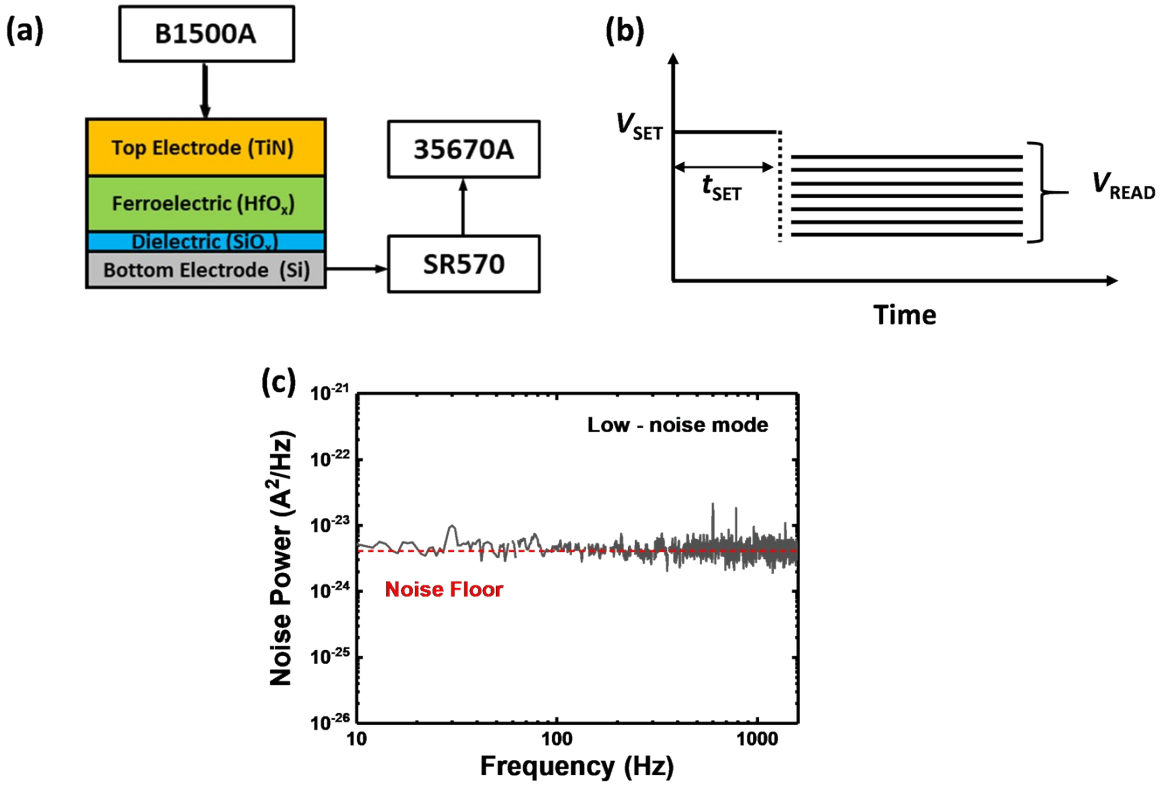

Figure S2. (a) Measurement setup and (b) bias scheme for measuring the LFN characteristics of the FTJ. The LFN characteristics of the FTJ were measured using a semiconductor parameter analyzer (B1500A), low noise current amplifier (SR570), and signal analyzer (35670A). The voltage applied to the TiN was supplied by the B1500A. The output current of the FTJ was connected to the SR570, converting the current fluctuation into a voltage fluctuation. 35670A converts the dynamic signal from SR570 to a power spectral density. (c) Noise floor of the measurement setup.

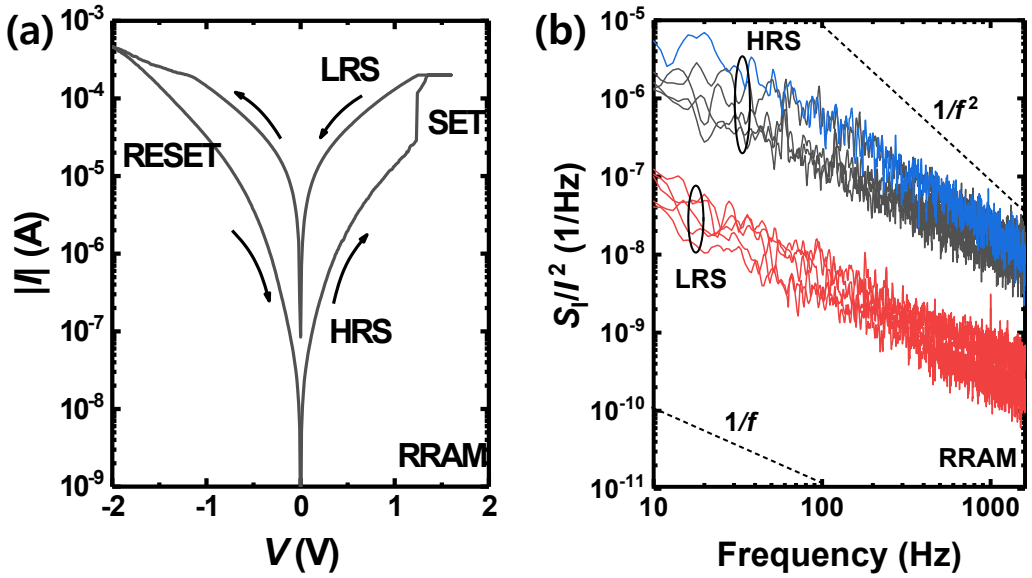

Figure S3. (a) Current-voltage ($|I|$-V) curve of the RRAM having HfO_x as a conductive channel. (b) Normalized current power spectral density (S_I/I^2) of the RRAM in the LRS (red lines) and HRS (black lines). The blue line denotes the random telegraph noise behavior of the RRAM in the HRS

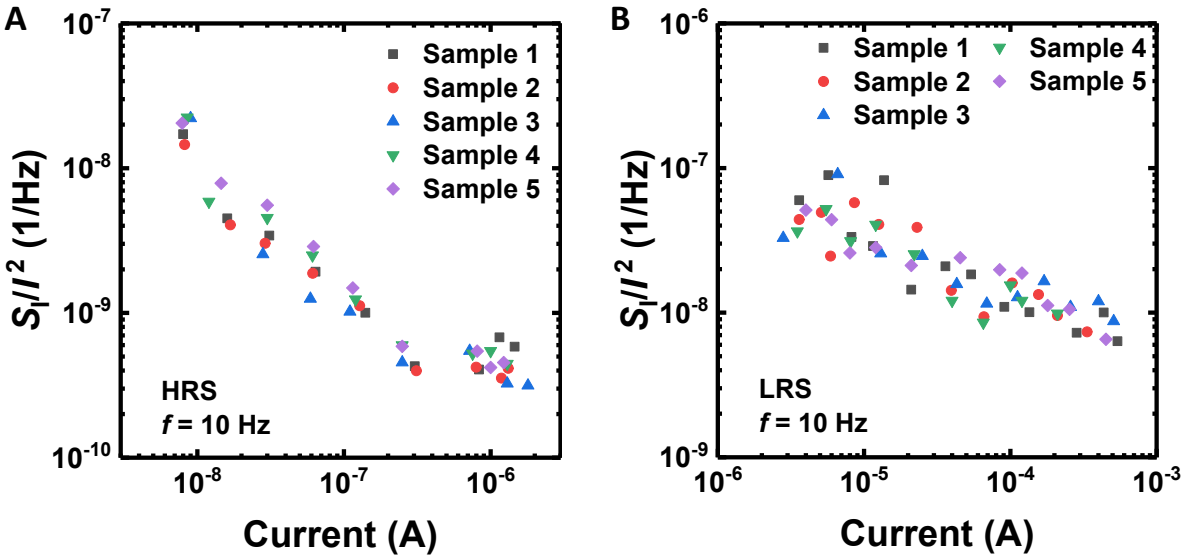

Figure S4. Normalized current power spectral density (S_I/I^2) versus current of the 5 independent FTJs in the (a) HRS and (b) LRS. The averaged value of the measured power spectral density is shown at Figures 3(c) and 4(b).

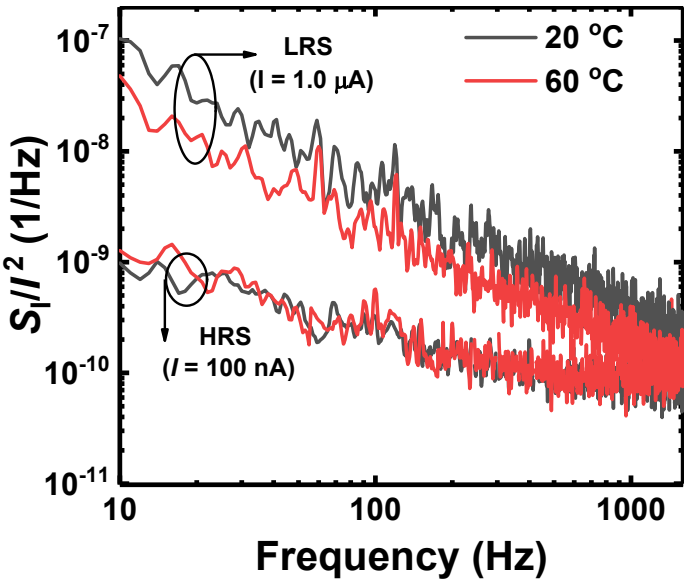

Figure S5. Normalized current power spectral density (S_I/I^2) of the FTJ in the LRS and HRS at 20 °C (black lines) and 60 °C (red lines).

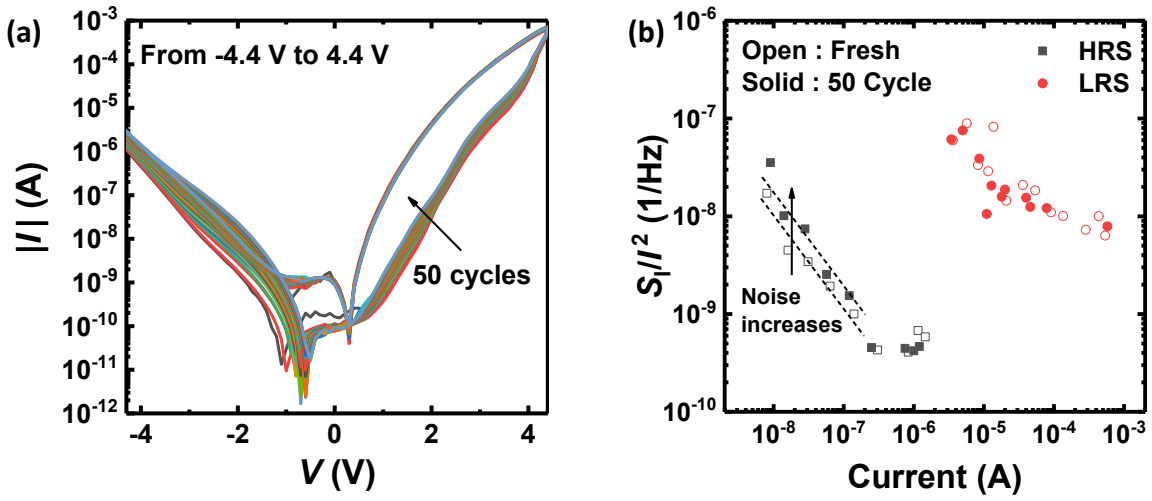

Figure S6. (a) Hysteresis curve ($|I|$-V) of the FJT with respect to 50 cycles of DC stress from -4.4 V to 4.4 V. (b) Normalized current power spectral density (S_I/I^2) versus current of the FTJ in the HRS and LRS before and after the 50 cycles of the DC stress.

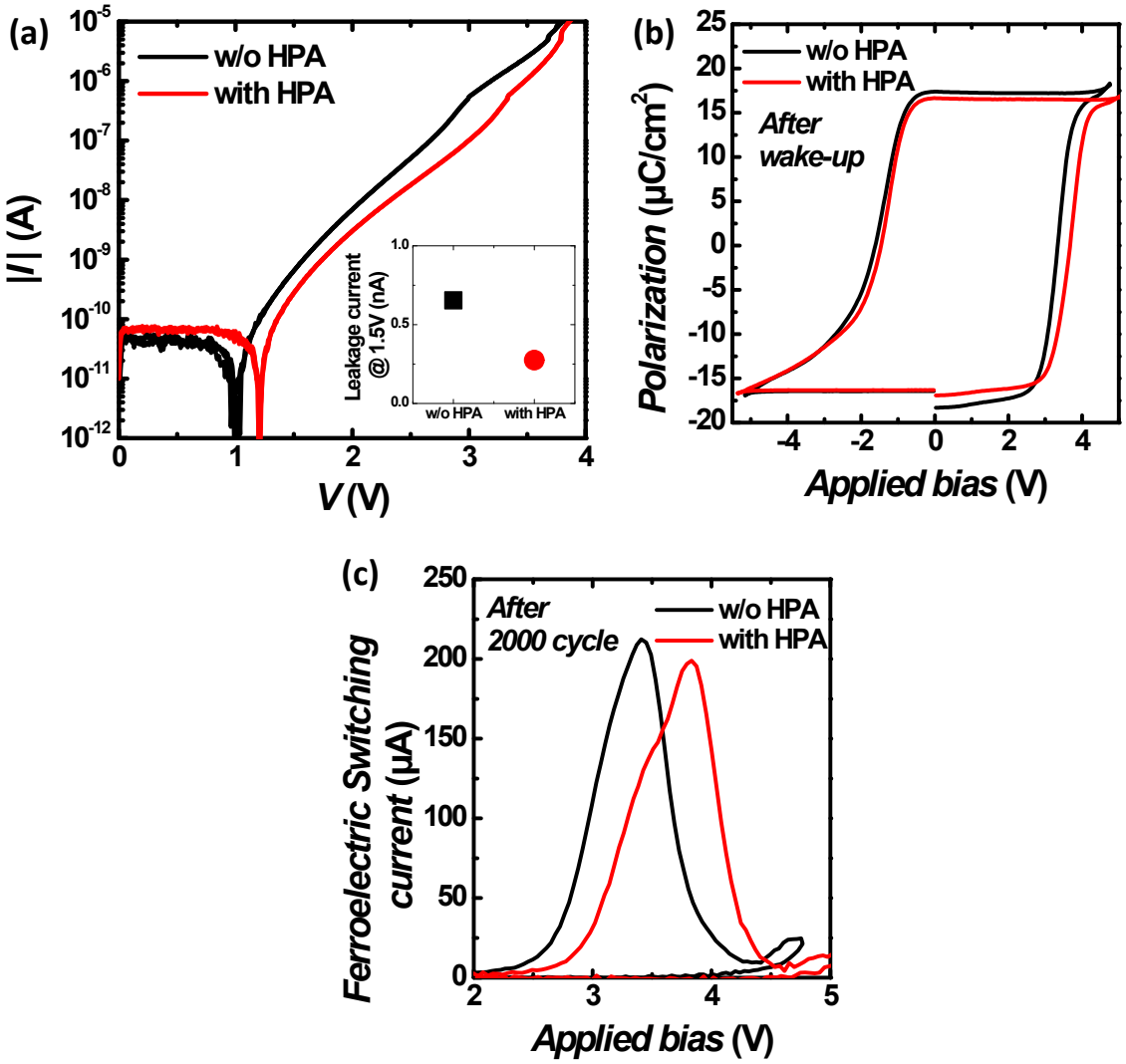

Figure S7. (a) Leakage current vs. applied voltage curves depend on HPA. The inset shows leakage current value extract at the 1.5V applied bias. (b) Polarization versus applied bias curve of with and without HPA. The wake-up procedure was completed before PUND measurement in each sample. (c) Ferroelectric switching current versus applied bias curve after 2000 cycle is applied.